A TEM in situ study of the softening of Tungsten by Rhenium

Daniel Caillard

A TEM in situ study of the softening of Tungsten by Rhenium

Daniel Caillard [1]

1-**CEMES-PPM - Physique de la Plasticité et Métallurgie -** CEMES 29 rue Jeanne Marvig, BP 94347, F-31055 Toulouse Cedex 4 - France

Abstract

Transmission electron microscopy in situ straining experiments have been carried out in a W-8% Re alloy, between 100K and 300K, in order to determine the origin of softening by alloying with Re. The geometry and kinetics of glide show that Re solutes do not induce any change of main slip plane. The only clearly visible effect of Re is the pinning of screw dislocations at super-jogs, which should a priori induce some hardening, but which in fact has only a weak effect. Local measurements of the applied shear stress at the scale of individual dislocations nevertheless confirm that softening is well reproduced in the micro-samples. It is thus concluded that softening results from a decrease of the strength of Peierls valleys with respect to pure W.

1 - Introduction

When alloyed with rhenium, tungsten exhibits a pronounced increase of ductility which is of fundamental importance for many applications. According to Raffo et al [1], Raffo [2], Klopp [3] and Luo [4], this increased ductility is effective at room temperature, and more generally below 540K, namely in the temperature domain where the plasticity is expected to be controlled by a Peierls mechanism acting on screw dislocations.

This increase of ductility is presumably due to a decrease of the strain-hardening coefficient, coupled with a possible decrease of the yield stress. The experimental results are however not enough complete and not fully coherent. First, at increasing Re content up to 9%, and for a <100> tensile axis, Garfinkle [5] reports an increase of the flow stress at 0.2% of deformation, but a decrease of the same stress above 1% of deformation, as a result of a decrease of the

strain-hardening coefficient. This is partly corroborated by experiments of Raffo [2] carried out in polycrystalline alloys with up to 25% of Re, showing that ~~that~~ the strain hardening coefficient decreases with increasing Re content, and that the corresponding yield stress decreases[1]. Lastly, Stephens [6] reports in single crystals strained along <137>, a small decrease of the flow stress between 0.2% and 2% of strain, without any notable decrease of strain-hardening rate, but only for Re contents up to 3%.

We may thus consider that the effect of rhenium is rather weak at concentrations lower than 3%, and large between 3% and 25%. It is clearly connected to a decrease of the strain-hardening coefficient, at least for the investigated straining directions, and to either an increase or a decrease of the flow stress, depending on the corresponding amount of strain (below or above 1%).

This conclusion is supported by indentation experiments of Luo et al [4] showing that the softening effect is maximum at 4%Re.

Such a behavior is difficult to discuss with respect to the expected rate-controlling microscopic mechanism, namely the Peierls mechanism on screw dislocations. In alloys with large Re concentrations, the very sharp yield point followed by a rather flat stress-strain curve may correspond to the activation of the Peierls mechanism. However, the rather low deformation stress at 0.1% of strain, and the very strong strain hardening observed in pure W (except for the <110> orientation, see the discussion on {112} slip below) and in W-Re with less than 3%Re, are more difficult to interpret. In particular, the stress corresponding to the onset of ~~of~~ the Peierls mechanism appears difficult to determine unambiguously on account of the high strain-hardening in pure W and very dilute W-Re alloys.

[1] However, since the corresponding amount of strain was not given, this decrease of yield stress is difficult to compare with the results of Garfinkle, except if the so-called yield stress was measured at a strain higher than 1%.

This problem has been extensively discussed by Brunner [7], in pure W strained along a <149> direction. This author considers that since edge dislocations are much more mobile than screw ones, the deformation stress at low strain (e.g. 0.1%) is mainly controlled by the motion of the longest edge segments trailing immobile screw dipoles. Then, there should be a progressive exhaustion of these available edge segments, and the deformation stress should increase and reach the level necessary to make screw dislocations enough mobile. This exhaustion hardening mechanism is moreover amplified by the elasticity of the straining machine, which absorbs part of the applied strain-rate, and makes the plastic strain-rate lower than the applied one. Under such conditions, the increasing deformation stress can be identified as the stress necessary to deform the material at an increasing effective strain-rate (e.g. the stress to activate the Peierls mechanism at an increasing dislocation velocity). The stress necessary to move the screw dislocations at the velocity corresponding to the applied strain-rate is thus the deformation stress at several percent of strain, where the strain-hardening coefficient has strongly decreased[2].

The behavior of W with large amounts of Re (larger than 3%) is different because the early motion of edge dislocations is inhibited by static ageing due to the segregation of Re atoms. Edge and screw dislocations are then simultaneously mobile at a high stress corresponding to the sharp yield point.

According to this analysis, we can conclude that what we call the elastic limit, namely the stress necessary to move screw dislocations, must be measured at several percent of strain in pure W and very dilute W-Re alloys, and either just after the yield point or at several percent of strain (same result) in W with concentrations of Re larger than 3%. This stress is clearly decreased by the addition of large concentrations of Re.

[2] This stress is also that measured in the so-called ISTL tests of Brunner [7].

This review of the available experimental results can be completed by several microstructural observations, namely i) the high density of anchoring points on screw dislocations upon Re addition [6], and ii) the possible increased activity of {112} slip. The latter point (ii) results from experiments of Garfinkle [5] in W-5%-9% Re single crystals strained along a <100> direction, Stephens [6] in W-3%Re single crystals strained along a direction in the center of the unit triangle, and Li et al [8] in micro-cantilevers of W-26%Re.

The observation of {112} slip in W-Re alloys has led to speculations about the effect of Re in W. In particular, Garfinkle [5] pointed out the analogy between the stress-strain curves in pure W with a <110> axis, where extensive {112} slip has been observed [9, 10], and those in W-Re alloys where the same {112} slip has been observed. Indeed, in both cases the stress-strain curves exhibit a sharp yield point followed by a flat part with a rather low strain-hardening. Different models based on this observation of {112} slip will be described below. However, we can already remark that the presumed increase of {112} slip upon Re addition is not so obvious, because i) slip line observations are not numerous, and ii) the activation of {112} slip in pure W is strongly orientation dependent [9, 10] whereas only a few orientations of the straining axis have been investigated in W-Re. It is thus a priori exaggerated to conclude that Re promotes a change of slip plane from {110} to {112}.

The various interpretations for the effect of Re in W are based on two main hypotheses, i) the decrease of the stress necessary to overcome the Peierls valleys, by the classical kink-pair mechanism, and ii) the change of slip plane from {110} to {112}.

The decrease of the activation energy to nucleate a pair of kinks at the vicinity of a solute Re atom has been calculated by several methods. It is the subject of a wide consensus, for Re concentrations of 12% and 25%, see e.g. Romaner et al [11], Li et al [8], Samolyuk et al [12], Hu et al [13] (all DFT calculations), and Zhao and Marian [14] (kinetic Monte Carlo). Similar

results have been obtained by DFT calculations in other bcc metals (Mo) by Trinkle and Woodward [15], and Medveda et al [16].

This effect is sometimes accompanied by a change of the core configuration, from symmetric and compact in pure W, to asymmetric or degenerated in W-Re, see e.g. [8, 11, 12] (Re concentrations of 12-25%), but not in all cases [13]. Such a change of core structure could be at the origin of the change of main slip plane, but not the real cause of the softening effect, according to [11]. We must however remember that the connection between core structure and slip plane is not so straightforward, because {112} and {123} slip have been clearly observed in pure W where screw dislocations have a compact core [9, 10].

The aim of this paper is thus to investigate the properties of moving dislocations in a W-8% Re alloy, by means of in situ straining experiments, and to i) check a possible increase of {112} slip with respect to pure W, ii) try to measure a possible decrease of the strength of the Peierls mechanism at the scale of individual dislocations, and iii) compare the effect of Re in W to that of several substitutional solute atoms like Si in Fe, published earlier [17]. In situ straining experiments allow one to directly observe the behavior of dislocations under stress at different temperatures, determine the strongest (controlling) obstacles to their movement, measure several important parameters like dislocation velocity as a function of local stress, friction stress, etc., and get rid of the exhaustion mechanisms at yield by working at constant dislocation velocity instead of constant applied strain-rate.

2 - Experimental

The W-8%Re alloy has been provided by J.P. Couzinié, CNRS-ICMPE in Thiais, France. It has been prepared by arc melting under Ar atmosphere using raw metals (slugs and wire) with purity exceeding 99.9 wt.%. The alloy has melted five times and the small ingot has been flipped between each step to ensure chemical homogeneity. Microsamples with the shape of

small rectangles have been cut by spark erosion, mechanically polished, and electro-polished until the formation of a thin edged hole at their center. They have been subsequently glued on a copper grid and strained in a JEOL 2010 HC transmission electron microscope, using a Gatan low-temperature straining holder. The grain size is large enough to make grain boundary effects negligible, and the as-grown dislocation density is low enough to observe easily the first steps of dislocation motion and multiplication. The images were recorded by a Megaview III camera and analyzed frame by frame. The investigated grains are oriented and analyzed in three dimensions using different tilt angles and diffracting conditions. More details about the procedure, the advantages and limitations of the method, can be found in a preceding article devoted to pure tungsten [10].

3- Experimental results

3-1 General observations

Fig. 1 shows the same active slip band at 100K, 200K, and 300K. The average slip plane is close to (110), in a grain with surface plane $(0\bar{1}2)$ and straining axis [321], and the dislocations moving from right to left have a $1/2[1\bar{1}1]$ Burgers vector. At 100K, the dislocations are very straight along their screw direction, as in pure W. However, as the temperature increases to 200K and 300K, the dislocations become more and more curved between pinning points noted P, where they often trail edge dipoles noted dp. These dipoles subsequently close up and form prismatic loops noted lo, visible as dark dots in (b) and (c). This behavior is very different from that observed previously in pure W [10], where no pinning is observed, but similar to that observed in concentrated Fe-Si and Fe-Cr alloys [17]. The corresponding mechanism will be detailed in what follows, but we can already notice that pinning points usually produce hardening at variance from the softening mechanism investigated in this study.

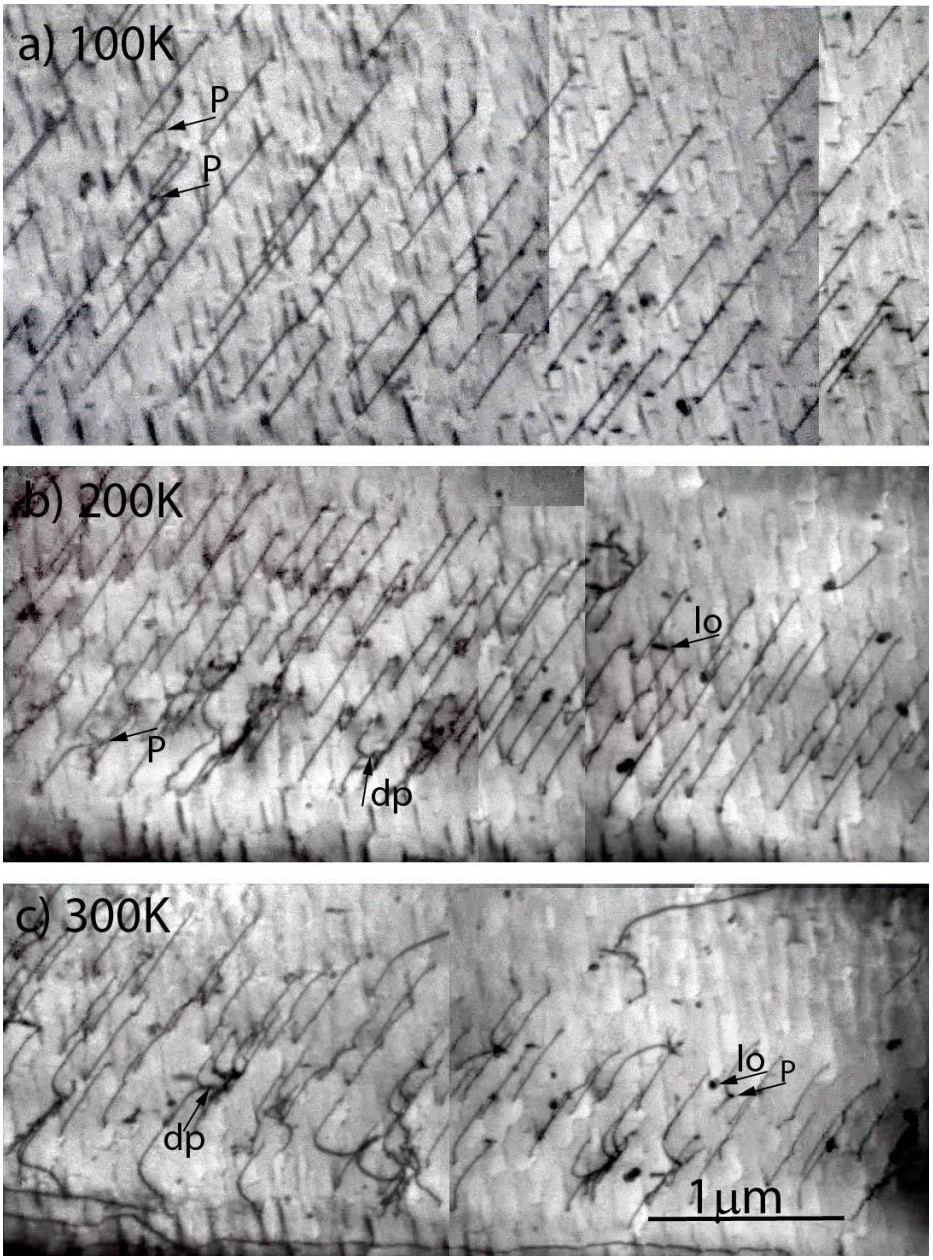

Fig. 1: Same area of an active slip band at increasing temperatures (a) 100K, (b) 200K, and (c) 300K. P refer to pinning points, dp to edge dipoles formed at some pinning points, and lo to prismatic loops.

Figs. 2 and 3 show how these dislocations glide, at respectively 100K and 300K. The images (b) to (d) are differences between images taken at an interval of 0.24s or 0.12s. At 100K (fig. 2), they show a rather slow and steady motion of straight screw segments 1 to 3, typical of a Peierls controlling mechanism. In (d), dislocation 2 has not moved over its whole length, which means that it has been pinned at its lower part. At 300K (fig. 3), the motion of another

set of dislocations 1 to 3 is a little bit faster and more irregular (i.e. not at a constant velocity), but since these dislocations remain straight and screw along a large fraction of their length, their motion appears still controlled the Peierls mechanism.

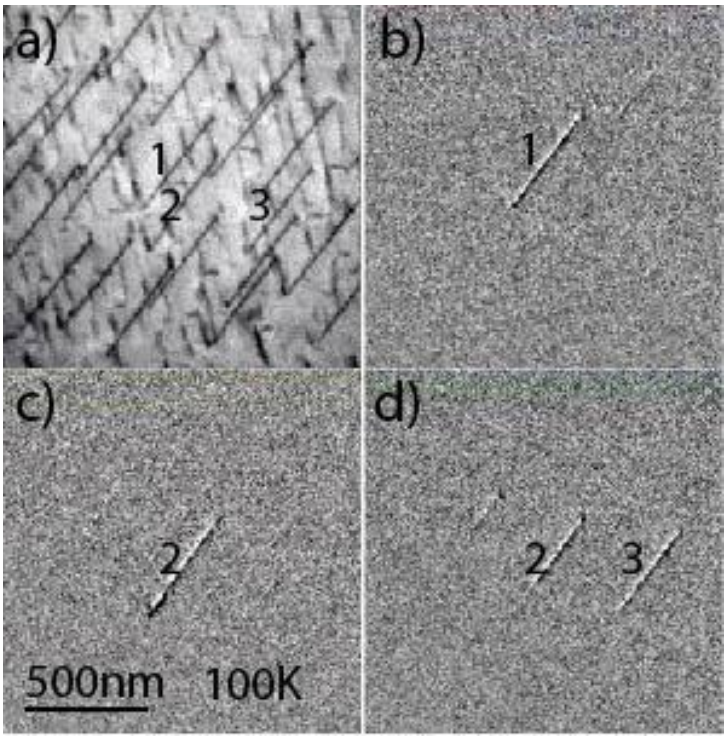

Fig. 2: Kinetics of screw dislocation motion at 100K, in the band of fig. 1 (a). (b) to (d) are differences between video frames taken at time intervals of 0.24s. They show the slow motion of dislocations 1-3. See the corresponding video as a supplementary material.

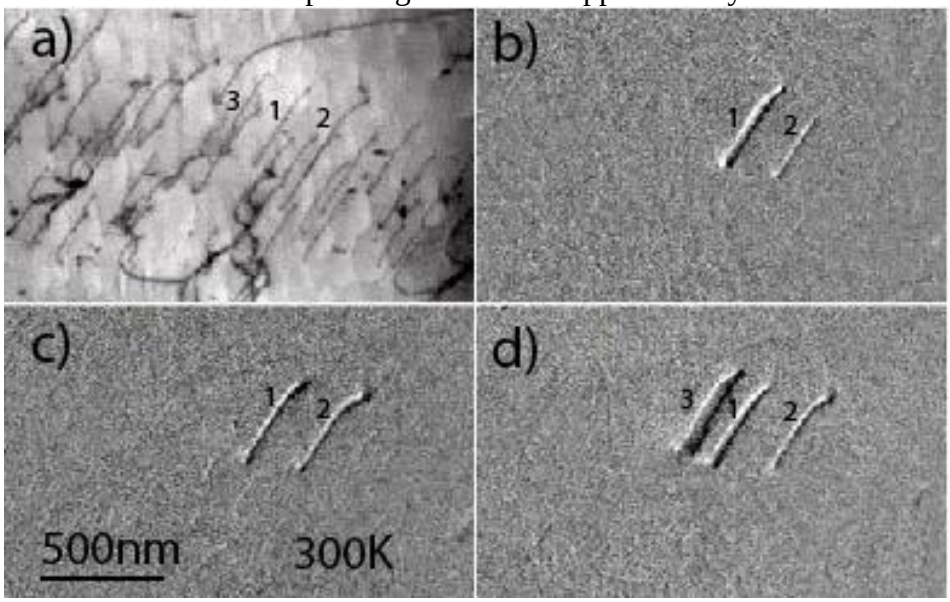

Fig. 3: Kinetics of screw dislocation motion at 300K, in the band of fig. 1 (c). (b) to (d) are differences between video frames taken at time intervals of 0.12s. They show the slow motion of dislocations 1-3. See the corresponding video as a supplementary material.

According to [17], the pinning points are super-jogs formed by a "cross-kink mechanism" at the vicinity of solute atoms. These super-jogs can glide laterally along the Burgers vector direction, but since they are sessile in the direction of motion, they are nevertheless efficient pinning points. Fig. 4 shows how these super-jogs are formed at 300K, and how they produce prismatic loops. A screw dislocation S moving to the top-left in (a) is pinned at a super-jog noted sj, in (b). After a further motion of the lower screw part S_1, an edge dipole dp is formed in (c). Then, the dipole closes up and forms a prismatic loop lo which subsequently glides upwards in the direction of the Burgers vector (arrow). Images (e)-(g) are the differences of images (a)-(d).

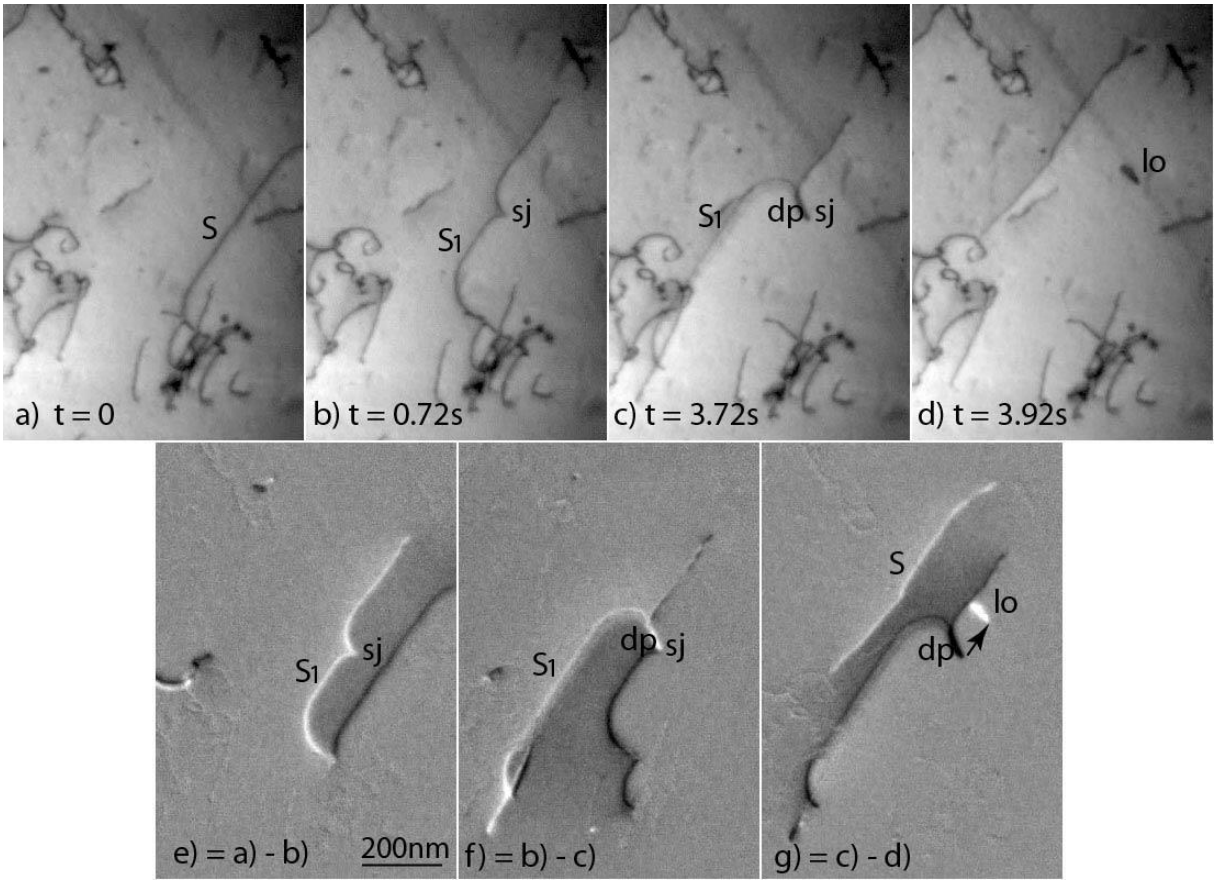

Fig. 4: Glide motion of a screw dislocation S at 300K. The dislocation is pinned at a super-jog sj in (b). The super-jog is by-passed and a dipole dp is trailed in (c). The dipole closes up and forms a prismatic loop lo gliding in its cylinder in (d). The sample plane is $(2\bar{1}6)$, the

(vertical) tensile axis is [$\bar{3}$01], and the Burgers vector is 1/2 [$\bar{1}$11]. See the corresponding video as a supplementary material.

Fig. 5 shows a similar mechanism at 200K, namely the lateral glide of a dipole dp formed at the super-jog sj, as a result of the glide motion of the upper part S_1 of a screw dislocation (images (a) and (b)). Like the prismatic loop in fig. 4, the dipole subsequently glides in the direction of the Burgers vector (image (c), arrow in the difference-image (d)).

Lastly, fig. 6 shows the same process at 100K. A screw dislocation anchored at the super-jog sj trails a dipole dp after the motion of its upper part S_1 to the left. The dipole then expands and forms two opposite screw segments (arrowed in image (d))

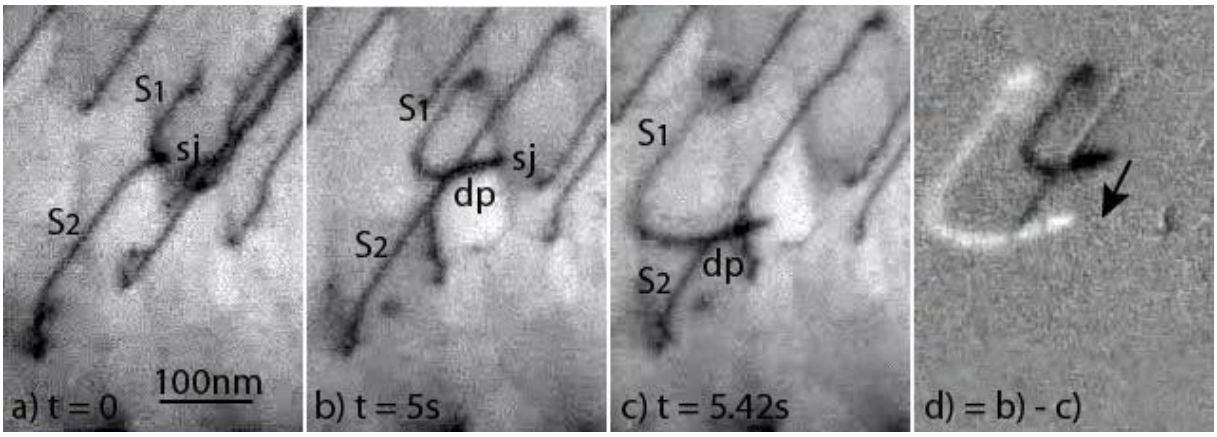

Fig. 5: Glide motion of a screw dislocation S at 200K. The dislocation is pinned at a super-jog sj in (a). It goes on moving and trails a dipole dp in (b). The dipole glides downwards in the Burgers vector direction in (c). Same sample as in figs. 1 to 3. See the corresponding video as a supplementary material.

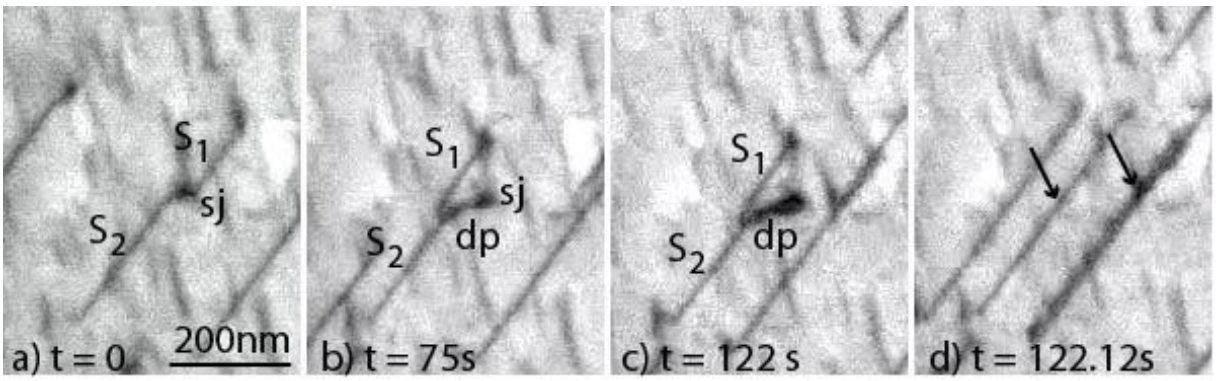

Fig. 6: Glide motion of a screw dislocation S at 100K. The dislocation is pinned at a super-jog sj in (a). It goes on moving and trails a dipole dp in (b, c). Then, the dipole expands and forms two straight screws arrowed in (d). Same sample as in figs 1-3 and 5. See the corresponding video as a supplementary material.

It is interesting to note that although the screw dislocations in figs. 4-6 are strongly pinned at super-jogs, they (at least one of their two halves noted S_1) never stop but go on gliding at a velocity still controlled by the Peierls mechanism. Then, the obstacle is easily by-passed with no waiting time. This is possible because these screw segments remain straight over a substantial part of their length, in such a way that the nucleation of kink pairs is never inhibited, even when the curvature near the anchoring point is very pronounced. Under such conditions, as discussed in [17], super-jogs are not very efficient obstacles against the motion of screw dislocations, and what seems to be a strong hardening mechanism is in reality almost inoperative. This point will be discussed further in section 4.

3-2 Slip planes

Elementary slip planes can in principles be determined when their intersections with the sample surfaces (called slip traces) are sufficiently straight over long distances to be attributed to single slip. The slip plane is then the plane containing the trace and the Burgers vector of the gliding dislocation. In many cases, however, slip traces are wavy as a result of frequent cross-slip between elementary slip planes which cannot be easily identified.

Fig. 7 to 9 show several favorable situations where slip planes can in principles be unambiguously determined.

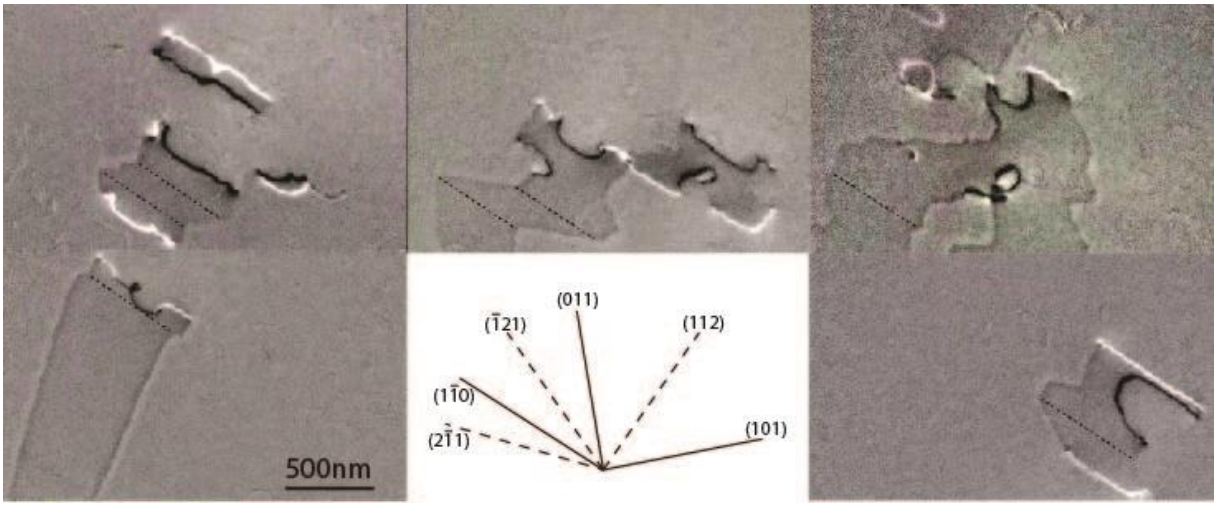

Fig. 7: Slip traces trailed by mobile screws at 300K (difference-images between different frames of the video). The traces exhibit straight segments corresponding to none of the possible {110} and {112} slip planes. The foil plane is (001), the vertical tensile axis is $[\overline{5}10]$, and the Burgers vector is $1/2[\overline{1}\overline{1}1]$.

Fig. 7 is a compilation of gliding dislocations trailing pairs of slip traces on the two sample surfaces. The traces are typical of stair-shaped glide surfaces with straight segments possibly indicating elementary slip planes, and stair rods parallel to the Burgers vector $1/2[\overline{1}\overline{1}1]$ (in projection). However, we find no exact agreement between these slip trace directions and those expected in case of slip in various {110} and {112} planes containing the Burgers vector. This may be interpreted as slip in {123} planes, as in pure W strained along a <110> direction [10], but with no absolute certainty.

Fig. 8 shows an example of slip in a {110} plane at 300K, at a dislocation source with a single anchoring point S. Two dislocation segments rotate clockwise around S and trail slip traces at the two foil surfaces. This situation is especially favorable to determine the active slip planes because, as discussed in [18], we are absolutely sure that kinks cannot be nucleated at the free sample surfaces during the rotation around S[3]. In other words, kink pairs are necessarily

[3] This results from two properties, i) the clockwise rotation around the pinning point increasing the dislocation length during the motion, in such a way that surface nucleation of single kinks would not be energetically favorable, and ii) the dislocation curvature at the free surfaces (due to some surface anchoring) preventing the

nucleated in the sample interior as in a bulk material. Here, the two slip traces close to S are not strictly parallel because of a wedged sample shape, but they unambiguously indicate planar slip in the (101) plane containing the 1/2[$\bar{1}$11] Burgers vector. Away from the source, the emitted dislocations cross slip onto the edge-on (110) plane as a result of thin foil effects discussed elsewhere [18-20]. A similar behavior at the vicinity of a single-ended source has been described in details in figs. 8 and 9 of reference [18].

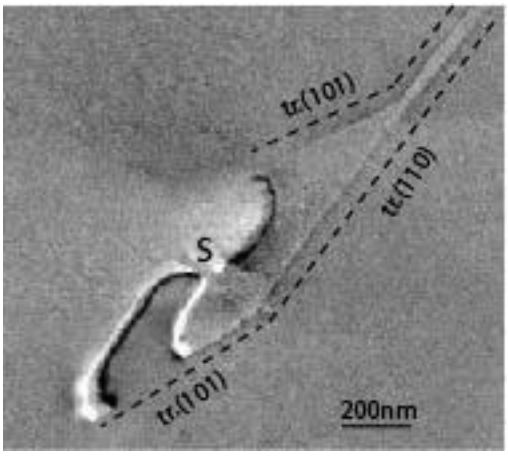

Fig. 8: Single-ended dislocation source at 300K (difference between two frames separated by 0.18s). Two dislocation arms rotate clock-wise around the pinning point S, glide in (101) and cross slip in (110) away from the source. The geometry prevents from any surface-induced kink-nucleation (see text). Same sample and same Burgers vector as in fig. 4. See the corresponding video as a supplementary material.

Fig. 9 shows an example of slip in a {112} plane in the same sample at 300K, at another dislocation source very similar to the preceding one. Here again, kinks cannot be nucleated at the free surfaces and the dislocation is expected to behave as in the bulk material. The slip traces are not easily visible but they can be materialized by the superposition of successive positions of the rotating dislocation, in the composite image fig. 9c. The dislocation with Burgers vector 1/2[$\bar{1}$11] glides exactly in the (211) plane, in the twinning direction.

direct emergence of the straight screw parts. See fig. 16 of reference [19] and figs. 8 and 9 of reference [20] for a more complete discussion.

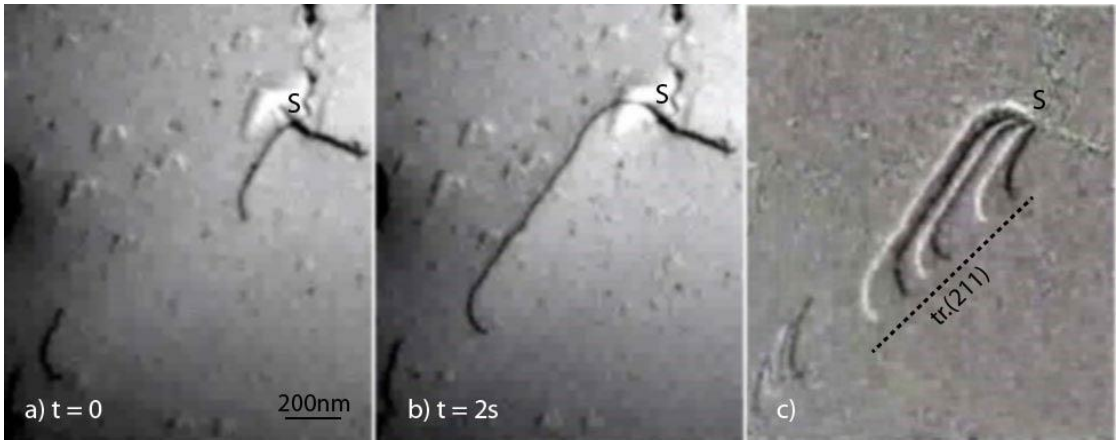

Fig. 9: Single-ended dislocation source at 300K. The dislocation arm rotates clockwise around the pinning point S and glides in (211). (c) is a compilation of difference-images showing several positions of the dislocations in bright and dark. Same sample and Burgers vector as in figs. 4 and 8. See the corresponding video as a supplementary material.

These various observations show that both {110}, {112} and possibly other high-index slip planes like {123} are likely to operate as elementary[4] slip planes in W-8%Re. Since all these slip planes have also been observed at the scale of individual dislocations in pure W [10], we can conclude that there is no obvious change of main slip plane after alloying with rhenium. As in pure W, {110}, {112} or {123} elementary slip planes are likely to be active in various proportions, probably as a function of the orientation of the straining axis.

3-3 Local stress measurements

Contrary to pure metals, but like in Fe-Si investigated in [17], the measurement of the local shear stress acting on moving dislocations is rather difficult. In pure metals, curved dislocations not subjected to any friction stress start to move as soon as the applied shear stress τ_a overcomes the line tension stress τ_l holding them back. This yields the equation $\tau_a = \tau_l = T/Rb$, where R is the radius of curvature, T is the line tension, and b is the Burgers vector. Alternatively, we can use in pure W the formulae τ_a (MPa) = $\tau_l = 23.7\ 10^3\ (b/d_c)\ln(d_c/b)$,

[4] i.e. not resulting from intensive cross-slip between other planes

where d_c is the critical width of an expanding screw dipole, the term $\ln(d_c/b)$ reflects the dependence of the line tension T on the outer cut-of radius taken equal to d_c, and the proportionality term is deduced from anisotropic elasticity calculations [10]. The critical width d_c can be measured with a fairly good accuracy in pure W, because the expansion is very fast as soon as energetically favorable, as a result of a very large difference between edge and screw mobility. Then, reliable values of the applied shear stress can be obtained [10, 21].

In concentrated alloys, the situation is more complex because dislocations (especially those with a large edge component) are subjected to a friction stress τ_f resulting from their interaction with solute atoms. Then, the equilibrium equation $\tau_a = \tau_l$ must be replaced by $\tau_a - \tau_f = \tau_l$, with τ_l still equal to $23.7\ 10^3\ (b/d_c)\ln(d_c/b)$. This has two bad consequences, i) the experimental values of τ_l are more scattered because τ_f is not rigorously constant, and ii) τ_a cannot be determined unless τ_f can be precisely estimated.

Figs. 10 and 11 show two expanding dipoles, at 300K and 100K. The dipole in fig. 10 expands progressively at an increasing width d_c, which illustrates the smaller difference between edge and screw velocities with respect to pure W, and the difficulty of measuring a reliable value of d_c. The slip trace on fig. 10d is slightly serrated, which means that the curved non-screw part has moved by pencil glide on a wavy surface. We can nevertheless define an average slip trace noted tr and a corresponding average dipole plane. Fig. 11 shows the same process at 100K with a smaller d_c. The critical widths have been measured at various temperatures, and the results (after geometrical corrections accounting for the tilt angle of the average dipole plane) are plotted in fig. 12, at 100K and 300K. They yield $\tau_l = \tau_a - \tau_f =$ 360MPa at 100K, 270MPa at 200K, 210MPa at 250K, and 120MPa at 300K.

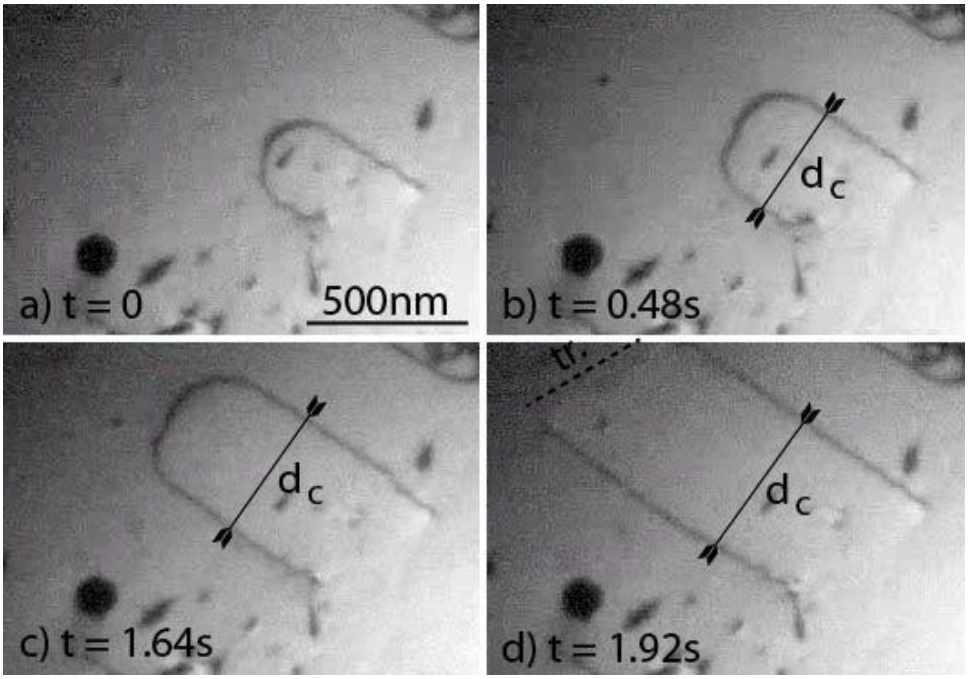

Fig. 10: Expansion of a screw dipole at 300K. The curved non-screw part moves rather slowly to the top-left at an increasing value of the dipole width d_c. See the corresponding video as a supplementary material.

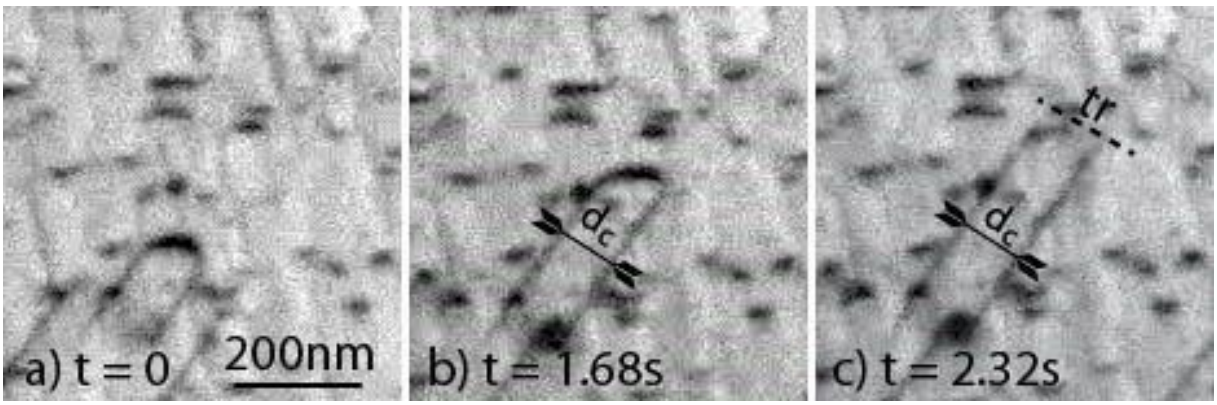

Fig. 11: Expansion of a screw dipole at 100K. The curved non-screw part moves rather slowly to the top-right at a slightly increasing value of dipole width d_c. See the corresponding video as a supplementary material.

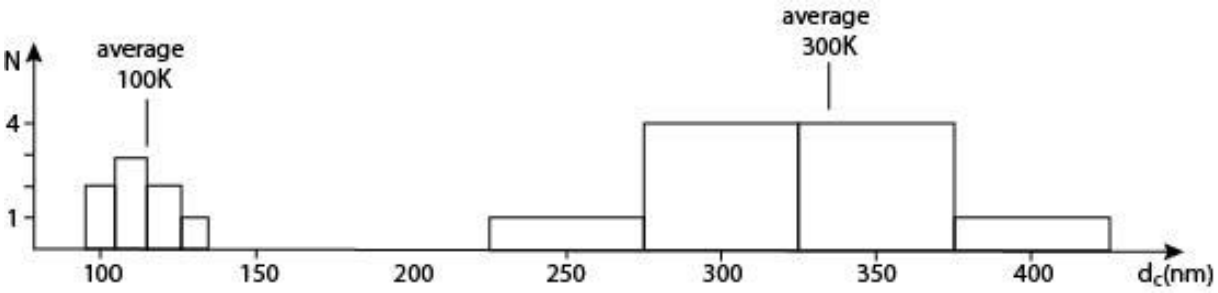

Fig. 12: Critical values of expanding dipole widths d_c, after correction from dipole tilt angle. N is the number of measurements corresponding to a given value of d_c, at 100K (left) and 300K (right).

Several methods to estimate τ_f are now proposed and compared, in order to give reliable values of τ_a.

Fig. 13 shows a screw dislocation pinned at a super-jog noted sj (fig. 13a). Upon further straining, the left screw segment by-passes the super-jog (fig. 13b), the curved part moves to the right, emerges at the surface, and forms a screw dipole of width d (fig. 13c). Depending on the value of d (corrected from perspective effects), such a dipole can either expand like in figs. 9 and 10, if d is large enough, or shrink if d is too small. This leads to the following situations:

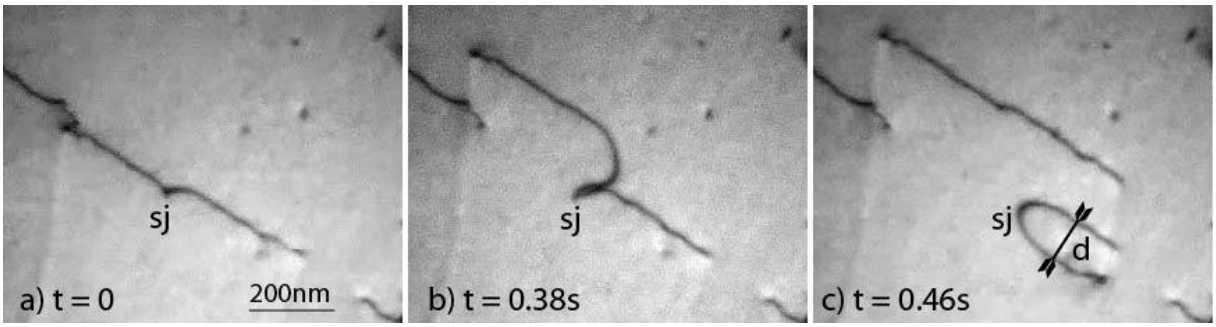

Fig. 13: Screw dislocation at 300K, pinned at a super-jog sj, in (a), by-passing the super-jog, in (b), and forming a dipole of width d, in (c). Same sample and dislocation Burgers vector as in fig. 7. See the corresponding video as a supplementary material.

i) Dipole of width d_s shrinking under stress. The equilibrium of forces can now be written $\tau_l(d_s) = \tau_a + \tau_f$, which, combined with the expansion condition $\tau_l(d_c) = \tau_a - \tau_f$, yields $\tau_a = [\tau_l(d_s) + \tau_l(d_c)]/2$, and $\tau_f = [\tau_l(d_s) - \tau_l(d_c)]/2$

ii) dipole of width d remaining stable under stress (case of fig. 13). The above equality becomes $\tau_l(d) < \tau_a + \tau_f$. If we find a large amount of such dipoles with a wide distribution of widths d, we can infer that the minimum of this distribution is only slightly above the critical shrinking value d_s.

iii) dipole of width d_s shrinking as a result of a partial release of the applied stress. The same equations as in (i) can be used with $\tau'_a < \tau_a$, which yields $\tau_a > [\tau_l(d_s) + \tau_l(d_c)]/2$, $\tau_f > [\tau_l(d_s) - \tau_l(d_c)]/2$, or $\tau_f > [\tau_l(d_s) - \tau_l(d_c)]/[\tau_l(d_s) + \tau_l(d_c)]$.

iv) locked or very slow pure edge dislocations under stress. This last method is based on the observation of long hardly mobile edge segments trailed by mobile screws, in the most concentrated alloys. In this case, we can infer that $\tau_{fe} \approx \tau_a$, where τ_{fe} is the friction on pure edge segments. Assuming that τ_f is proportional to the edge character of mixed segments, we can estimate the average friction stress on a curved half loop as $\tau_f \approx (2/\pi)\tau_{fe}$, whence $\tau_f \approx (2/\pi)\tau_a$.

None of these methods is fully convincing alone, but, provided they give consistent results, they can be used all together to obtain a fairly good order of magnitude of τ_f and τ_a.

Fig. 14 shows two screw dipoles belonging to the same dislocation, under stress at 100K. This complex structure, sometimes called “open loop” is not planar, but the two dipoles are in close slip planes. The widest dipole of width $d_c \approx$ 100nm expands between figs 14 (a) and (b) ($\tau_l(d_c) \approx$ 360MPa), whereas the narrowest one of width $d_s \approx$ 54nm shrinks ($\tau_l(d_s) \approx$

660MPa). Using the first criterion (i) we obtain $\tau_a \approx$ 510MPa and $\tau_f \approx$ 150MPa, namely $\tau_a \approx 0.3\tau_a$.

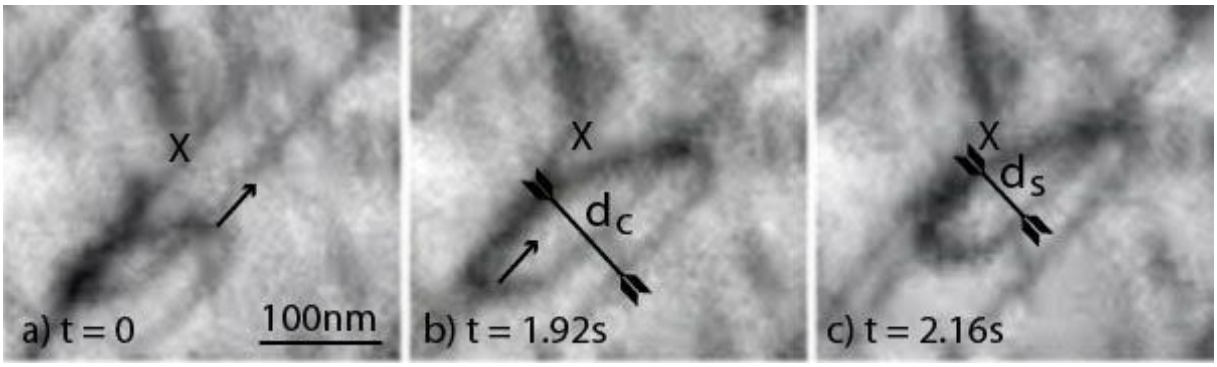

Fig. 14: Screw dislocation forming two opposite screw dipoles of widths d_c and d_s, both moving in the arrowed direction, at 100K. Same sample and dislocation Burgers vector as in figs. 1-3. See the corresponding video as a supplementary material.

Still at 100K, the third criterion (iii) applied to several other observations yields $\tau_a >$ 540MPa, $\tau_f >$ 180MPa, and $\tau_f > 0.33\tau_a$. The fourth one (iv) yields $\tau_a <$ 1000MPa, and $\tau_f < 0.64\tau_a$. We can thus conclude that $\tau_a \approx$ 500-550MPa, and $\tau_f \approx 0.30$-$0.35\tau_a$ at 100K.

At room temperature, the second criterion (ii) yields $\tau_a \approx$ 290MPa and $\tau_f \approx 0.58\tau_a$, and the fourth one (iv) yields $\tau_a \lesssim$ 340MPa and $\tau_f \lesssim$ 0.64MPa, whence $\tau_a \approx$ 300MPa and $\tau_f \approx 0.6\tau_a$.

The yield stress at room temperature $\tau_a \approx$ 300MPa is larger than that deduced from macroscopic tests at $\varepsilon \approx$ 3% by Garfinkle [5] ($\tau_a \approx$ 200MPa, with a Taylor factor of 2.5). According to [10], this is due to the shorter length of screw dislocations in thin foils, the so-called “smaller is stronger” effect. For instance, in pure W, yield stresses were observed to decrease from 740MPa to 500MPa (a value close to the macroscopic yield stress) in samples with various thicknesses increasing from 200nm to 600nm, where 600nm approximately corresponds to the transition between the small-size and the bulk behavior of pure W [10, 22].

However, the important point is that the in situ yield stress in W-8%Re is twice lower than that in pure W.

In the same way, the in situ yield stress at 100K (500-550MPa) is half that in pure W (950MPa according to [10]). This means that the softening effect of rhenium has been correctly reproduced in our micro-samples.

4- Discussion

The dislocation motion has almost similar properties between 100K and 300K, characterized by i) straight screw dislocations gliding slowly and steadily as a result of a Peierls controlling mechanism, ii) extensive cross-slip between elementary slip planes which can be of {110}, {112} and possibly {123} type, and iii) strong pinning at super-jogs resulting from a cross-kink mechanism at the vicinity of solute atoms described in [17].

In this respect, the observed dislocation behavior is very similar to that observed in Fe-Si alloys, in the low-temperature range of 100K-200K for Fe-1.3%Si, and 100K-150K for Fe-3%Si [17]. We observe the same difference between the pure metal (W or Fe) where screw dislocations are never pinned by super-jogs, and the alloys (Fe-Si or W-Re) where large densities of dipoles and prismatic loops are formed at super-jogs. Note that observations of dipoles and prismatic loops are in fairly good agreement with earlier observations of Stephens [6].

Still like in Fe-Si (in the low-temperature range), the pinning by super-jogs, although clearly visible, does not substantially hardens the material, because the yield stress remains controlled by the Peierls mechanism like in pure metals. In other words, the super-jogs are not efficient obstacles, because they are by-passed or recombined as a result of the continuous motion of the straight screw parts in-between them, controlled by the Peierls mechanism. At this step,

we thus find no hardening due to the addition of rhenium, and the origin of softening remains unexplained.

Still like in Fe-Si [17], a transition to a hardening effect is expected when the by-passing of super-jogs can be rate-controlling. This should occur well above room temperature, probably at 540K where the softening effect is replaced by a more classical hardening effect (see introduction). This should also occur close to room temperature, for larger Rhenium concentrations. We have unfortunately not made the corresponding experiments.

Softening is also probably not the result of any change of elementary slip planes, from {110} to {112}. Indeed, both types of planes (and also possibly {123} planes) are observed in pure W as well as in W-Re. In pure W, the occurrence of {112} is highly orientation dependent, and maximum for straining axes close to <110> [9, 10]. In W-Re, grains were randomly oriented, in such a way that no systematic investigation of the effect of straining axes could be made. Since a possible change of elementary slip plane from {110} to {112} is sometimes attributed to a change of core configuration, from compact to degenerated upon Re addition, we do not bring any argument in favor of such a change of core configuration. Note however that changes of core structure and corresponding slip planes have been predicted for rather large Rhenium concentrations of 12-25%, larger than the present one (8%).

Our stress measurements nevertheless show that softening is a real effect well reproduced in thin foils and at the scale of individual dislocations. Indeed, the yield stress necessary to move screw dislocations over large distances and to activate sources is almost twice lower than in pure W under similar conditions. As in pure W, this stress corresponds to the motion of individual screw dislocations over a Peierls potential, apart for any pile-up or other stress concentration effect. The softening effect must accordingly be attributed to a strong decrease of the strength of Peierls valleys, either in {110}, {112} or possibly {123} planes. We have thus provided an experimental validation of the calculations reported in the introduction. The

fact that the critical resolved shear stress necessary to overcome the Peierls potential is – like in pure W – almost the same in {110} and {112} planes remains unexplained.

5- Conclusions

Micro-samples of W-8%Re have been strained in situ in a TEM between 100K and 300K, in order to find the exact origin of softening by Re addition. The results are as follows:

- Straight screw dislocations glide slowly and steadily in {110} and {112} planes, and cross-slip intensively. No collective effect has been observed.
- Screw dislocations are anchored at super-jogs formed by a cross-kink mechanism at the vicinity of solute Re atoms. Like in Fe-Si strained at low temperature, these super-jogs do not however harden substantially the material in the temperature range considered
- Local measurements of the average friction stress on non-screw curved dislocations allow one to estimate the local shear stress. This shows that softening by Re addition is correctly reproduced in the micro-sample, at the scale of individual dislocations

These experimental results allow us to give the following conclusions:

- W-Re is markedly different from pure W where the deformation stress measured locally is much higher, and where no pinning by super-jogs is observed. W-Re is however very similar to Fe-Si strained below room temperature
- There is no substantial hardening due to dislocation anchoring at super-jogs in the temperature range investigated
- There is no enhanced {112} slip due to Re atoms. Both W-Re and pure W exhibit a mixture of {110} and {112} slip. Softening by Re addition is thus not the result of any change of elementary slip plane

- Softening does not result from any collective effect. Then, it necessarily results from a decrease of the stress to activate the Peierls mechanism, in agreement with recent atomistic calculations

Acknowledgements: The author is indebted to Jean-Philippe Couzinié and Loïc Perrière for the alloy preparation, and to Dominique Lamirault for the delicate micro-sample preparation. This work has been carried out within the framework of the EUROfusion Consortium and has received funding from the Euratom research and training program 2014-2018 under grant agreement No 633053. The views and opinions expressed herein do not necessarily reflect those of the European Commission.

References

[1] P.L. Raffo, W.D. Klopp, W.R. Witzke, Mechanical properties of arc-melted and electron-beam melted tungsten-base alloys, NASA Technical Note D-2561 (1965)

[2] P.L. Raffo, Yielding and fracture in tungsten and tungsten-rhenium alloys, J. of the Less-common Metals 17 (1969) 133-149.

[3] W.D. Klopp, Review of ductilizing of group VIA elements by rhenium and other solutes, NASA Technical Note D-4955 (1968)

[4] A. Luo, D.L. Jacobson, K.S. Shin, Solution softening mechanism of iridium and rhenium in tungsten at room temperature, Refractory Metals and Hard Materials 10 (1991) 107-114.

[5] M. Garfinkle, Room-temperature tensile behavior of <100> oriented tungsten single crystals with rhenium in dilute solid solution, NASA Technical Note D-3190 (1966).

[6] J.R. Stephens, Dislocation structures in single-crystal tungsten and tungsten alloys, Metallurgical Transactions 1 (1970 1293-1301.

[7] D. Brunner, Temperature dependence of the plastic flow of high-purity tungsten single crystals, Int. J. Mat. Res. 101 (2010) 1003-1013.

[8] H. Li, S. Wurster, C. Motz, L. Romaner, C. Ambrosch-Draxl, R. Pippan, Dislocation core symmetry and slip planes in tungsten alloys : ab-initio calculations and micro-cantilever bending experiments, Acta Mater. 60 (2012) 748-758.

[9] A.S. Argon, S.R. Maloof, Plastic deformation of tungsten single crystals at low temperatures, Acta Metall. 14 (1966) 1449-1462.

[10] D. Caillard, Geometry and kinetics of glide of screw dislocations in tungsten between 95K and 573K, Acta Mater. 161 (2018) 21-34.

[11] L. Romaner, C. Ambrosch-Draxl, R. Pippan, Effect of rhenium on the dislocation core structure in tungsten, Phys. Rev. Letters 104 (2010) 195503-1-4.

[12] G.D. Samolyuk, Y.N. Osetsky, R.E. Stoller, The influence of transition metal solutes on the dislocation core structure and values of the Peierls stress and barrier in tungsten, J. Phys : Condens. Mater. 25 (2013) 025403-1-9.

[13] Y.J. Hu, M.R. Fellinger, B.G. Bulter, Y. Wang, K.A. Darling, L.J. Kecskes, D.R. Trinkle, Z.K. Liu, Solute-induced solid-solution softening and hardening in bcc tungsten, Acta Mater. 141 (2017) 304-316.

[14] Y. Zhao, J. Marian, Direct prediction of the solute softening-to-hardening transition in W-Re alloys using stochastic simulations of screw dislocation motion, Modelling Simul. Mater. Sci. Eng. 26 (2018) 045002-1-15.

[15] D.R. Trinkle, C. Woodward, The chemistry of deformation: how solutes soften pure metals, Science 310 (2005) 1665-1667.

[16] N.I. Medvedeva, Y.N. Gornostyrev, A.J. Freeman, Electronic origin of solid solution softening in bcc molybdenum alloys, Physical Review Letters 94 (2005) 136402-1-4.

[17] D. Caillard, A TEM in situ study of alloying effects in iron – II solid solution hardening caused by high concentrations of Si and Cr, Acta Mater. 61 (2013) 2808-2827.

[18] D. Caillard, Kinetics of dislocations in pure Fe, part I, in situ experiments at room temperature, Acta Mater. 58 (2010) 3493-3503.

[19] D. Caillard, A TEM in situ study of alloying effects in iron - I solid-solution softening caused by low concentrations of Ni, Si and Cr, Acta Mater. 61 (2013) 2793-2807.

[20] D. Caillard, An in situ study of hardening and softening of iron by carbon interstitials, Acta Mater. 59 (2011) 4974-4989.

[21] D. Caillard, Kinetics of dislocations in pure Fe, part II, in situ experiments at low temperatures, Acta Mater. 58 (2010) 3504-3515.

[22] J. Y. Kim, D. Jang, J. R. Greer, Tensile and compressive behavior of tungsten, molybdenum, tantalum and niobium at the nanoscale, Acta Mater. 58 (2010) 2355-2363.